



Journal of Applied and Computational Mechanics



Research Paper

Buckling and Vibration Analysis of a Double-layer Graphene Sheet Coupled with a Piezoelectric Nanoplate

K. Malekzadeh Fard¹, M. Khajehdehi Kavanroodi², H. Malek-Mohammadi³,
A.R. Pourmoayed⁴

¹ Malek Ashtar University of Technology, Tehran, Iran, Email: kmalekzadeh@mut.ac.ir

² Department of Mechanical Engineering, Semnan University, Semnan, Semnan, Iran, Email: m.khajehdehi@semnan.ac.ir

³ Department of Mechanical Engineering, Bu-Ali Sina University, Hamedan, Hamedan, Iran, Email: hoseinmm15@gmail.com

⁴ Department of Mechanical Engineering, Khatmol Anbia Air Defense, Tehran, Iran, Email: pourmoayed@mut.ac.ir

Received January 03 2020; Revised February 22 2020; Accepted for publication March 10 2020.

Corresponding author: A.R. Pourmoayed (pourmoayed@mut.ac.ir)

© 2022 Published by Shahid Chamran University of Ahvaz

Abstract. In this article, the vibration and buckling of a double-layer Graphene sheet (DLGS) coupled with a piezoelectric nanoplate through an elastic medium (Pasternak and Winkler models) are investigated. DLGS are subjected to biaxial in-plane forces and van der Waals force existing between each layer. Polyvinylidene fluoride (PVDF) piezoelectric nanoplate is subjected to an external electric potential. For the sake of this study, sinusoidal shear deformation theory of orthotropic plate expanded with Eringen's nonlocal theory is selected. The results indicate that nondimensional frequency and nondimensional critical buckling load rise when the ratio of width to thickness increases. Furthermore, incrementing the effect of elastic medium parameter results in increasing the stiffness of the system and, consequently, rising nondimensional frequency and critical buckling load.

Keywords: Double-Layer Graphene Sheets, Piezoelectric Nanoplate, Elastic Medium, Sinusoidal Shear Deformation Theory, Nonlocal Piezoelectricity Theory.

1. Introduction

Recently, nanomaterials and nanostructures have had several applications in various nano-devices, micro-electro-mechanical-systems (MEMS), nano-electro-mechanical-systems (NEMS) such as strain sensor and mass and pressure sensor, and regarding their superior electrical and mechanical properties, they have attracted the attention of scientific community [1,2]. Polyvinylidene fluoride (PVDF) is a piezoelectric polymer, which has unique properties, such as excellent dimensional stability, abrasion and corrosion resistance, high strength, and capability of maintaining its mechanical properties at elevated temperature [3]. On the other hand, Graphene is composed of a flat monolayer tightly compacted carbon atom into a two-dimensional honeycomb lattice. Graphene also has premier properties, which include high mechanical strength, large thermal conductivity, and excellent electric conductivity [4-6].

Eringen states that classical (local) theories will give acceptable responses when the ratio of external characteristic of length to internal characteristic of length is substantial. However, when this ratio approximates one, classical (local) theories do not present an accurate response, so the small scale effect must be considered in this case. Thus, in contrast to the classical theory which considers the stress of one point as a function of strain at that point, Eringen's nonlocal theory, which is one type of the continuum mechanical theories dependent on size, states that stress at one point is a function of strain at all points of continuum [7-9].

Ghorbanpour Arani et al. [10] and Pradhan and Kumar [11] investigated the vibration of coupled DLGS embedded on Visco-Pasternak foundation and single-layer Graphene sheets (SLGS) using nonlocal classical plate theory, respectively. Ghorbanpour Arani et al. [12] analyzed the buckling and smart control of SLGS using nonlocal Mindlin plate theory and observed that the buckling load ratio decreases when the nonlocal parameter rises. Ke et al. [13] examined free vibration of nonlocal piezoelectric nanoplates under various boundary conditions applying nonlocal Mindlin plate theory and found out that frequency decreases when electric voltage increases. Damping vibration of smart piezoelectric polymeric nanoplate by nonlocal strain gradient theory was analyzed by Ebrahimi and Barati [14]. Shen et al. [15] investigated the vibration of SLGS using nonlocal Kirchhoff plate theory. Malekzade et al. [16] analyzed the small scale effect on free vibration of orthotropic nanoplate applying nonlocal first order shear deformation theory and concluded that nondimensional frequency rises when limitation in nanoplate edges increases. Pradhan and Phadikar [17] examined nonlocal vibration of nanoplate using nonlocal classical plate theory and nonlocal first order shear deformation plate theory. Malikan [18] investigated the buckling of composite plate with nano coating, based on the modified couple stress theory. Zhu and Li investigated [19] the twisting static behaviors of through-radius functionally graded nanotubes



by formulating a nonlocal integral model, based on Eringen's nonlocal integral elasticity. In another article, Zhu and Li [20] study the size-dependent effect on the dispersion relation and vibration frequencies using single-walled carbon nanotube, single layer graphene sheet and silicon as nanoscaled rods, which can show a good agreement with molecular dynamics results or experimental data. Allahyari and Asgari [21] analyzed thermo-mechanical vibration of double-layer Graphene sheets via nonlocal third order shear deformation plate theory. Kadari et al. [22] investigated the buckling of orthotropic nanoplate by using hyperbolic plate theory and nan-local small scale effects. In Shaat's [23] article a general nonlocal theory and its approximations for slowly varying acoustic waves is under consideration and this general nonlocal theory is reduced to the strain gradient theory and the couple stress theory. Ghorbani et al. [24] determined carbon nanotubes size-dependent parameters, which are molecular dynamics simulation and nonlocal strain gradient continuum shell model. In their article, nonlocal and material length scale parameters are calibrated by comparing the natural frequencies obtained from MD simulation and nonlocal strain gradient theory. Thai et al. [25] investigated the vibrations and buckling of SLGS applying nonlocal sinusoidal shear deformation theory stated by Touratier [26]. Khajehdehi et al. [27] analyzed the buckling of DLGS coupled with another DLGS by Pasternak medium considering surface stress effect. Ghorbanpour Arani et al. [28] and Zenkour and Sobhy [29] analyzed electro-magneto wave propagation of viscoelastic sandwich nanoplates of ZnO-SLGS-ZnO and the thermal buckling of SLGS laying on Winkler-Pasternak elastic medium, using sinusoidal shear deformation theory, respectively. Chemi et al. [30] assessed nonlocal critical buckling loads of chiral double-walled carbon nanotubes embedded in an elastic medium implementing nonlocal Timoshenko beam theory. Narendar and Gopalakrishnan [31] investigated the scale effects on the buckling of orthotropic SLGS based on nonlocal two-variable refined plate theory and found out that nondimensional critical buckling load of orthotropic nanoplate is less than that of isotropic nanoplate. Lindahl et al. [32] investigated the values of bending rigidity of double-layer Graphene membranes, experimentally, using the snap-through behavior of convex buckled Graphene membranes under the electrostatic pressure. Pradhan [33] analyzed the buckling of SLGS based on nonlocal elasticity and higher order shear deformation theory.

With respect to the usage of the DLGS coupled with a piezoelectric nanoplate in nano-electro-mechanics, nano-sensors, nano-switches, etc., and regarding the huge expenses and the complexity of doing nano scale experiments, developing continuum mechanical theories for analyzing the mechanical behavior of nanostructures is desirable. In the present study, an analysis of the vibration and buckling of DLGS coupled with a PVDF piezoelectric nanoplate through an elastic medium is performed. The elastic medium is simulated according to Pasternak and Winkler models. Each Graphene layer is subjected to a biaxial in-plane force and under van der Waals force due to the other Graphene layer, and the bottom layer of Graphene is under forces caused by the elastic medium, and PVDF nanoplate is subjected to an external electric potential and also forces caused by the elastic medium. In the study, sinusoidal shear deformation theory of orthotropic plate developed by Eringen's nonlocal theory is applied. Governing relations and equations are obtained using Hamilton's principle. Simply supported boundary conditions of the all four edges of nanoplates are assumed for the system; thus, governing relations are solved applying Navier method. Nondimensional critical buckling load and nondimensional frequency of the system are obtained based on several parameters such as nonlocal parameter, external electric voltage, various ratios of length to width and width to thickness, different modes and various biaxial compression ratios. Some results for the system are obtained considering ZnO nanoplate rather than PVDF nanoplate and the results of the two systems are compared.

2. Basic Equation

2.1 Nonlocal Theory

Based on nonlocal piezoelectricity theory, the stress and electric displacement field of a particular point depend not only on strain and electric field components at the same point but also on all other points of the body. The nonlocal theory can be stated as nonlocal constitutive behavior [3, 5]:

$$\begin{aligned} (1 - (e_0 \bar{a})^2 \nabla^2) \sigma_{ij}^{nl} &= \sigma_{ij}^l \\ (1 - (e_0 \bar{a})^2 \nabla^2) D_{ij}^{nl} &= D_{ij}^l \end{aligned} \quad (1)$$

where σ_{ij}^{nl} and σ_{ij}^l show nonlocal stress tensor and local stress tensor, respectively. D_{ij}^{nl} and D_{ij}^l indicate components of nonlocal and local electric displacement, respectively. $\mu = (e_0 \bar{a})^2$ is the small-scale effect on the response of structures at nanosize and ∇^2 , \bar{a} , e_0 represent the Laplacian operator, internal characteristic length of the material and constant appropriate to each material, respectively. The nonlocal parameter depends on the boundary conditions, chirality, mode shapes, number of walls, and type of motion. So far, there is no rigorous study made on estimating the value of the nonlocal parameter. It is suggested that the value of nonlocal parameter can be determined by experiment or by conducting a comparison of dispersion curves from the nonlocal continuum mechanics and molecular dynamics simulation [25].

2.2 Sinusoidal shear deformation plate theory

The sinusoidal (higher-order) shear deformation theory (SSDPT) develops the first-order theory by considering shear strain and consequently shear stress not to be constant through the plate thickness and also the shear correction factor considered in first order and Mindlin plate theories is not required anymore. The displacement field of the sinusoidal theory of plates is expressed as follows [25, 34]:

$$u_1(x, y, z, t) = u(x, y, t) - z \partial w / \partial x + h / \pi \sin(\pi z / h) \phi_x \quad (2a)$$

$$u_2(x, y, z, t) = v(x, y, t) - z \partial w / \partial y + h / \pi \sin(\pi z / h) \phi_y \quad (2b)$$

$$u_3(x, y, z, t) = w(x, y, t) \quad (2c)$$

where u , v , w are displacements at one point in the middle of a plate along the x , y , z coordinate, respectively, ϕ_x and ϕ_y are rotations from the middle surface along x and y directions, respectively, and h is the plate thickness.

By eqs. (2), the following linear strains are concluded:



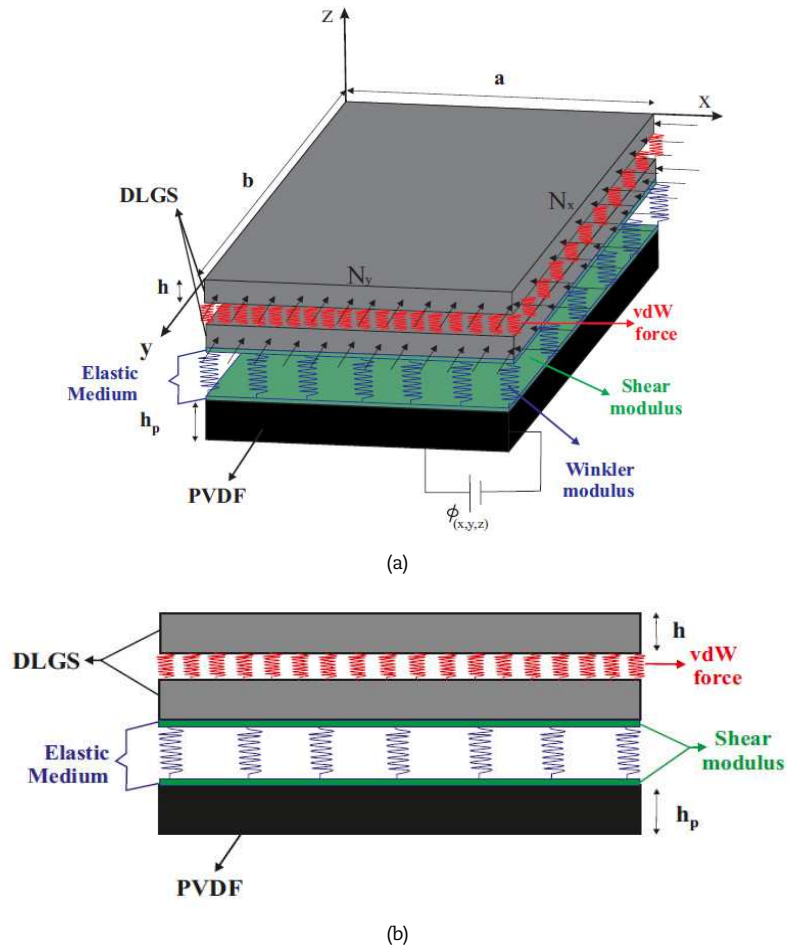


Fig. 1. DLGS coupled by an elastic medium (Pasternak and Winkler models) with PVDF nanoplate

$$\epsilon_x = \frac{\partial u}{\partial x} - z \frac{\partial^2 w}{\partial x^2} + \frac{h}{\pi} \sin\left(\frac{\pi z}{h}\right) \frac{\partial \phi_x}{\partial x} \tag{3a}$$

$$\epsilon_y = \frac{\partial v}{\partial y} - z \frac{\partial^2 w}{\partial y^2} + \frac{h}{\pi} \sin\left(\frac{\pi z}{h}\right) \left(\frac{\partial \phi_x}{\partial y} + \frac{\partial \phi_y}{\partial x} \right) \tag{3b}$$

$$\gamma_{xy} = \frac{\partial u}{\partial y} + \frac{\partial v}{\partial x} - 2z \frac{\partial^2 w}{\partial x \partial y} + \frac{h}{\pi} \sin\left(\frac{\pi z}{h}\right) \left(\frac{\partial \phi_x}{\partial y} + \frac{\partial \phi_y}{\partial x} \right) \tag{3c}$$

$$\gamma_{xz} = \cos(\pi z / h) \phi_x \tag{3d}$$

$$\gamma_{yz} = \cos(\pi z / h) \phi_y \tag{3e}$$

In eqs. (3), it is shown that the transverse shear strains (γ_{yz} , γ_{xz}) are zero, at the top ($z = h/2$) and bottom ($z = -h/2$) of the plate surfaces.

3. Governing Equations of Motion

Consider a DLGS system coupled with a piezoelectric nanoplate, as shown in Fig. 1, which contains geometric parameters of length a , width b , Graphene thickness h and PVDF thickness h_p . DLGS is coupled with PVDF through an elastic medium simulated based on Pasternak and Winkler. DLGS are subjected to biaxial in-plane forces and PVDF under electric potential.

The following matrix is the expanded form of nonlocal sinusoidal shear deformation orthotropic plate theory of DLGS [27]:

$$\begin{bmatrix} \sigma_x \\ \sigma_y \\ \sigma_{yz} \\ \sigma_{xz} \\ \sigma_{xy} \end{bmatrix} = \frac{1}{(1 - \mu \nabla^2)} \begin{bmatrix} C_{11} & C_{12} & 0 & 0 & 0 \\ C_{21} & C_{22} & 0 & 0 & 0 \\ 0 & 0 & C_{44} & 0 & 0 \\ 0 & 0 & 0 & C_{55} & 0 \\ 0 & 0 & 0 & 0 & C_{66} \end{bmatrix} \begin{bmatrix} \epsilon_x \\ \epsilon_y \\ \gamma_{yz} \\ \gamma_{xz} \\ \gamma_{xy} \end{bmatrix} \tag{4}$$



where C_{ij} are elastic coefficients,

$$\begin{aligned} C_{11} &= \frac{E_1}{1 - \nu_{12}\nu_{21}}, & C_{22} &= \frac{E_2}{1 - \nu_{12}\nu_{21}}, \\ C_{12} &= C_{21} = \nu_{12}C_{22} = \nu_{21}C_{11}, \\ C_{44} &= \tilde{G}_{12}, & C_{55} &= \tilde{G}_{23}, & C_{66} &= \tilde{G}_{13}, \end{aligned} \tag{5}$$

where E_1 and E_2 are Young's modules, G_{12}, G_{23} and G_{13} are shear modules, and ν_{12} and ν_{21} are Poisson ratios. The following matrix is the expanded form of nonlocal sinusoidal shear deformation orthotropic plate theory of PVDF:

$$\begin{bmatrix} \sigma_{xx} \\ \sigma_{yy} \\ \sigma_{yz} \\ \sigma_{xx} \\ \sigma_{xy} \\ D_{xx} \\ D_{yy} \\ D_{zz} \end{bmatrix} = \frac{1}{(1 - \mu \nabla^2)} \begin{bmatrix} C_{11}^p & C_{12}^p & 0 & 0 & 0 & 0 & 0 & -e_{31} \\ C_{21}^p & C_{22}^p & 0 & 0 & 0 & 0 & 0 & -e_{32} \\ 0 & 0 & C_{44}^p & 0 & 0 & 0 & -e_{24} & 0 \\ 0 & 0 & 0 & C_{55}^p & 0 & -e_{15} & 0 & 0 \\ 0 & 0 & 0 & 0 & C_{66}^p & 0 & 0 & 0 \\ 0 & 0 & 0 & e_{15} & 0 & \epsilon_{11} & 0 & 0 \\ 0 & 0 & e_{24} & 0 & 0 & 0 & \epsilon_{22} & 0 \\ e_{31} & e_{32} & 0 & 0 & 0 & 0 & 0 & \epsilon_{33} \end{bmatrix} \begin{bmatrix} \epsilon_{xx} \\ \epsilon_{yy} \\ \gamma_{yz} \\ \gamma_{xx} \\ \gamma_{xy} \\ E_{xx} \\ E_{yy} \\ E_{zz} \end{bmatrix} \tag{6}$$

where C_{ij}^p , e_{ij} and ϵ_{ii} are elastic, piezoelectric and dielectric coefficients. E_i is electric field in terms of electric potential (Φ) is obtained as follows [3,12]:

$$E_i = -\nabla\Phi = -\frac{\partial\Phi}{\partial i}, \quad i = x, y, z \tag{7}$$

The electric potential distribution in the thickness direction of the PVDF nanoplate as the combination of a half cosine and linear variation which satisfies the Maxwell equation is given as follows:

$$\Phi(x, y, z, t) = -\cos\left(\frac{\pi z}{h_p}\right)\varphi(x, y, t) + \frac{2zV_0}{h_p}e^{i\omega t} \tag{8}$$

4. Hamilton's Principle

Hamilton's principle is applied to obtain system energy and governing equations. The principle is adopted as follows [13, 35]:

$$\int_0^T (\delta U - \delta T - \delta K) dt = 0 \tag{9}$$

where δU , δT and δK denote the variations of strain energy, external work energy and kinetic energy, respectively.

The variations of strain energy for PVDF nanoplate are as follows, and not considering D_{xx} , D_{yy} and D_{zz} , the variations of strain energy for DLGS can be obtained.

$$\begin{aligned} & \int_{-h/2}^{h/2} (\sigma_x \delta \epsilon_x + \sigma_y \delta \epsilon_y + \sigma_{xy} \delta \gamma_{xy} + \sigma_{xz} \delta \gamma_{xz} + \sigma_{yz} \delta \gamma_{yz} - D_{xx} \delta E_{xx} - D_{yy} \delta E_{yy} - D_{zz} \delta E_{zz}) dAdz \\ & \int [N_x \frac{\partial \delta u}{\partial x} - M_x \frac{\partial^2 \delta w}{\partial x^2} + P_x \frac{\partial \delta \phi_x}{\partial x} + N_y \frac{\partial \delta v}{\partial y} - M_y \frac{\partial^2 \delta w}{\partial y^2} + P_y \frac{\partial \delta \phi_y}{\partial y} + N_{xy} \left(\frac{\partial \delta u}{\partial y} + \frac{\partial \delta v}{\partial x} \right) \dots \\ & \dots - 2M_{xy} \frac{\partial^2 \delta w}{\partial x \partial y} + P_{xy} \left(\frac{\partial \delta \phi_x}{\partial y} + \frac{\partial \delta \phi_y}{\partial x} \right) + Q_{xz} \delta \phi_x + Q_{yz} \delta \phi_y] dA \dots \\ & \dots - \frac{h}{2} \left[D_{xx} \left(\cos\left(\frac{\pi z}{h_p}\right) \frac{\partial \delta \varphi}{\partial x} \right) + \left[D_{yy} \left(\cos\left(\frac{\pi z}{h_p}\right) \frac{\partial \delta \varphi}{\partial y} \right) - \left[D_{zz} \left(\frac{\pi}{h_p} \sin\left(\frac{\pi z}{h_p}\right) \right) \delta \varphi + \frac{2V_0}{h_p} \right] \right] dAdz \end{aligned} \tag{10}$$

where N, M, P and Q are the stress resultants and are defined as follows. However, it should be noted that Graphene thickness and relation (4) are used for DLGS and piezoelectric nanoplate thickness and relation (8) are applied in stress resultants relations.

$$N_i = \int_{-\frac{h}{2}}^{\frac{h}{2}} \sigma_i dz, \quad (i = x, y, xy) \tag{11a}$$

$$M_i = \int_{-\frac{h}{2}}^{\frac{h}{2}} z \sigma_i dz, \quad (i = x, y, xy) \tag{11b}$$

$$P_i = \int_{-\frac{h}{2}}^{\frac{h}{2}} \frac{h}{\pi} \sin\left(\frac{\pi z}{h}\right) \sigma_i dz, \quad (i = x, y, xy) \tag{11c}$$

$$Q_i = \int_{-\frac{h}{2}}^{\frac{h}{2}} \cos\left(\frac{\pi z}{h}\right) \sigma_i dz, \quad (i = xz, yz) \tag{11d}$$



The variations of kinetic energy of the system are defined as follows:

$$\begin{aligned} \delta K = & \frac{h}{2} (\dot{u}_1 \delta \dot{u}_1 + \dot{u}_2 \delta \dot{u}_2 + \dot{u}_3 \delta \dot{u}_3) \rho dA dz = \int [I_0 (\dot{u} \delta \dot{u} + \dot{v} \delta \dot{v} + \dot{w} \delta \dot{w}) \dots \\ & \dots - I_1 \left(\dot{u} \frac{\partial \delta \dot{w}}{\partial x} + \frac{\partial \dot{w}}{\partial x} \delta \dot{u} + \dot{v} \frac{\partial \delta \dot{w}}{\partial y} + \frac{\partial \dot{w}}{\partial y} \delta \dot{v} \right) + I_2 \left(\frac{\partial \dot{w}}{\partial x} \frac{\partial \delta \dot{w}}{\partial x} + \frac{\partial \dot{w}}{\partial y} \frac{\partial \delta \dot{w}}{\partial y} \right) \dots \\ & + J_0 (\dot{u} \delta \dot{\phi}_x + \dot{\phi}_x \delta \dot{u} + \dot{v} \delta \dot{\phi}_y + \dot{\phi}_y \delta \dot{v}) \\ & \dots - J_1 \left(\frac{\partial \dot{w}}{\partial x} \delta \dot{\phi}_x + \frac{\partial \dot{w}}{\partial y} \delta \dot{\phi}_y + \dot{\phi}_x \frac{\partial \delta \dot{w}}{\partial x} + \dot{\phi}_y \frac{\partial \delta \dot{w}}{\partial y} \right) + K_0 (\dot{\phi}_x \delta \dot{\phi}_x + \dot{\phi}_y \delta \dot{\phi}_y)] dA \end{aligned} \quad (12)$$

where ρ is mass density and $I_0, I_1, I_2, J_0, J_1, K_0$ are mass inertia [25]:

$$I_0, I_1, I_2 = \int_{-\frac{h}{2}}^{\frac{h}{2}} \rho (1, Z, Z^2) dz = \rho h, 0, \frac{\rho h^3}{12} \quad (13a)$$

$$J_0, J_1 = \int_{-\frac{h}{2}}^{\frac{h}{2}} \rho (1, z) \frac{h}{\pi} \sin\left(\frac{\pi z}{h}\right) dz = 0, \frac{2\rho h^3}{\pi^3} \quad (13b)$$

$$K_0 = \int_{-\frac{h}{2}}^{\frac{h}{2}} \rho \left[\frac{h}{\pi} \sin\left(\frac{\pi z}{h}\right) \right]^2 dz = \frac{\rho h^3}{2\pi^2} \quad (13c)$$

The variations of external work energy are calculated with respect to multi-layer Graphene and van der Waals relations [4, 36] and elastic medium (Pasternak and Winkler models) relations as follows [5, 37, 38]:

$$T_1 = c_{12} (w_1 - w_2) \quad (14a)$$

$$T_2 = c_{21} (w_2 - w_1) - K_{23} (w_2 - w_3) + G_{23} \nabla^2 (w_2 - w_3) \quad (14b)$$

$$T_3 = -K_{32} (w_3 - w_2) + G_{32} \nabla^2 (w_3 - w_2) \quad (14c)$$

In-plane forces applied to DLGS and electric forces applied to PVDF are considered as follows [39, 40]

$$\hat{N}_j = N_x^0 \frac{\partial^2 w}{\partial x^2} + N_y^0 \frac{\partial^2 w}{\partial y^2} + 2N_{xy}^0 \frac{\partial^2 w}{\partial x \partial y}, \quad j = 1, 2 \quad (15a)$$

$$\hat{N}_e = N_{xe}^0 \frac{\partial^2 w}{\partial x^2} + N_{ye}^0 \frac{\partial^2 w}{\partial y^2} + 2N_{xye}^0 \frac{\partial^2 w}{\partial x \partial y} \quad (15b)$$

where

$$N_x^0 = \gamma_1 N_{cr}, \quad N_y^0 = \gamma_2 N_{cr}, \quad N_{xy}^0 = 0 \quad (16a)$$

$$N_{xe}^0 = 2e_{13} V_0, \quad N_{ye}^0 = 2e_{23} V_0, \quad N_{xye}^0 = 0 \quad (16b)$$

Substituting δU , δK and δT relations into Hamilton's principle, and integrating by parts and collecting δu , δv , δw , $\delta \phi_x$, $\delta \phi_y$ coefficients, motion equations for each layer are stated as follows:

$$\delta u_i : \frac{\partial N_x}{\partial x} + \frac{\partial N_{xy}}{\partial y} = I_0 \ddot{u}_i \quad (17a)$$

$$\delta v_i : \frac{\partial N_{xy}}{\partial x} + \frac{\partial N_y}{\partial y} = I_0 \ddot{v}_i \quad (17b)$$

$$\delta w_i : \frac{\partial^2 M_x}{\partial x^2} + 2 \frac{\partial^2 M_{xy}}{\partial x \partial y} + \frac{\partial^2 M_y}{\partial y^2} + T_i + \hat{N} = I_0 \ddot{w}_i - I_2 \frac{\partial^2 \ddot{w}_i}{\partial x^2} + J_1 \frac{\partial \ddot{\phi}_{xi}}{\partial x} - I_2 \frac{\partial^2 \ddot{w}_i}{\partial y^2} + J_1 \frac{\partial \ddot{\phi}_{yi}}{\partial y} \quad (17c)$$

$$\delta \phi_{ix} : \frac{\partial P_x}{\partial x} + \frac{\partial P_{xy}}{\partial y} - Q_{xz} = -J_1 \frac{\partial \ddot{w}_i}{\partial x} + K_0 \ddot{\phi}_{ix} \quad (17d)$$

$$\delta \phi_{iy} : \frac{\partial P_{xy}}{\partial x} + \frac{\partial P_y}{\partial y} - Q_{yz} = -J_1 \frac{\partial \ddot{w}_i}{\partial y} + K_0 \ddot{\phi}_{iy} \quad (17e)$$

In the above relations, $i=1, 2, 3$ represents the number of the layers.



Graphene properties are used for the first and second layers, PVDF properties are applied for the third layer, and eqs. (15) are used for N of DLGS and PVDF nanoplates, respectively.

5. Solving with Navier Method

Navier method is used for obtaining critical buckling load and frequency of the system for all nanoplates with four edges simply supported boundary conditions. Navier method automatically satisfies boundary conditions of simply supported nanoplates [41-43]:

$$u_i = \sum_{m=1}^{\infty} \sum_{n=1}^{\infty} u_{imn} \cos \frac{m\pi}{a} x \sin \frac{n\pi}{b} y e^{j\Omega t} \tag{18a}$$

$$v_i = \sum_{m=1}^{\infty} \sum_{n=1}^{\infty} v_{imn} \sin \frac{m\pi}{a} x \cos \frac{n\pi}{b} y e^{j\Omega t} \tag{18b}$$

$$w_i = \sum_{m=1}^{\infty} \sum_{n=1}^{\infty} w_{imn} \sin \frac{m\pi}{a} x \sin \frac{n\pi}{b} y e^{j\Omega t} \tag{18c}$$

$$\phi_{ix} = \sum_{m=1}^{\infty} \sum_{n=1}^{\infty} \phi_{ixmn} \cos \frac{m\pi}{a} x \sin \frac{n\pi}{b} y e^{j\Omega t} \tag{18d}$$

$$\phi_{iy} = \sum_{m=1}^{\infty} \sum_{n=1}^{\infty} \phi_{iy mn} \sin \frac{m\pi}{a} x \cos \frac{n\pi}{b} y e^{j\Omega t} \tag{18e}$$

$$\varphi = \sum_{m=1}^{\infty} \sum_{n=1}^{\infty} \varphi_{mn} \sin \frac{m\pi}{a} x \sin \frac{n\pi}{b} y e^{j\Omega t}, \quad i = 1, 2, 3 \tag{18f}$$

where $j = \sqrt{-1}$ and Ω is natural frequency of the system.

Substituting eqs. (18) into eqs. (17), matrix equation of the system is obtained as follows:

$$\begin{aligned} & ([A]_{16 \times 16} - \Omega^2 [M]_{16 \times 16}) [U] = 0 \\ & [U] = [u_{imn} \ v_{imn} \ w_{imn} \ \phi_{ixmn} \ \phi_{iy mn} \ \varphi_{mn}]_{16 \times 1} \\ & (i = 1, 2, 3) \end{aligned} \tag{19}$$

where [A] is stiffness matrix, and [M] is mass matrix. The above Matrix elements are defined in ‘‘Appendix’’. And the other elements are zero.

6. Results and Discussion

In this section, nondimensional critical buckling load and nondimensional frequency of the system, with respect to matrix relation (19), are derived as eqs. (20) and (21) [41-44]:

$$N_0 = \frac{N_c a^2}{E_2 h^3} \tag{20}$$

$$\Omega_0 = \frac{\Omega a^2}{h} \sqrt{\frac{\rho_G}{E_2}} \tag{21}$$

The properties of material are listed in Table. 1. Geometric properties of nanoplates, external electric voltage, physical properties of elastic medium and van der Waals coefficient are as follows [12, 27, 43]:

$$\begin{aligned} h &= 0.34 \text{ nm}, h_p = 2 \text{ nm}, b = 20h, a = b, \\ V_0 &= 2 \text{ volt}, \\ G &= 2.71273 \frac{N}{m}, K = 8.9995035 \text{ Gpa} / \text{ nm}, \\ c &= -45 \text{ Gpa} / \text{ nm} \end{aligned} \tag{22}$$

6.1 Validation with other studies

The research is validated with similar studies in the field, in this part. Ghorbanpour Arani et al [12] analyzed the buckling of an SLGS coupled with a PVDF nanoplate using nonlocal Mindlin plate theory. Confirming the present study with that of Ghorbanpour Arani et al [12], that is, removing the first layer (top Graphene nanoplate) and considering geometric specifications of nanoplates, the two studies are compared and the results of comparing the ratio of buckling loads for the higher modes are shown in Fig. 2. Similar to the studies done by Pradhan and Kumar [11], Shen et al. [15] and Pradhan and Padikar [17], the results for the ratio of frequency are obtained considering a Graphene nanoplate of the system (i.e. removing one layer of double-layer Graphene nanoplate and also removing piezoelectric nanoplate and elastic medium). They utilized the properties of isotropic SLGS in their studies ($E = 1.06 \text{ TPa}$ and $\nu = 0.25$) and also considered geometric properties $a=b=10 \text{ nm}$. The results of the comparison are presented in Table 2. As observable in Figure 2 and Table 2, the study is of high accuracy.



Table 1. Material properties of DLGS, PVDF and ZnO [3, 12, 28, 45]

DLGS	PVDF	ZnO
	$C_{11}^p = 238.24\text{Gpa}$	$C_{11}^p = 207\text{Gpa}$
	$C_{12}^p = C_{21}^p = 3.98\text{Gpa}$	$C_{12}^p = C_{21}^p = 117.7\text{Gpa}$
	$C_{22}^p = 23.60\text{Gpa}$	$C_{22}^p = 207\text{Gpa}$
	$C_{44}^p = 2.15\text{Gpa}$	$C_{44}^p = 44.8\text{Gpa}$
$E_1 = 1765\text{ Gpa}$	$C_{55}^p = 4.40\text{Gpa}$	$C_{55}^p = 44.6\text{Gpa}$
$E_2 = E_3 = 1588\text{ Gpa}$	$C_{66}^p = 6.43\text{Gpa}$	$C_{66}^p = 0.446\text{Gpa}$
$\nu_{12} = \nu_{13} = 0.3$	$e_{31} = e_{13} = -0.13\text{C} / \text{m}^2$	$e_{31} = e_{13} = -0.51\text{C} / \text{m}^2$
$\nu_{21} = \nu_{31} = 0.27$	$e_{32} = e_{23} = -0.145\text{C} / \text{m}^2$	$e_{32} = e_{23} = -0.51\text{C} / \text{m}^2$
$\nu_{32} = \nu_{23} = 0.27$	$e_{15} = e_{51} = -0.009\text{C} / \text{m}^2$	$e_{15} = e_{51} = -0.45\text{C} / \text{m}^2$
$\rho_G = 2250\text{kg} / \text{m}^3$	$e_{24} = e_{42} = -0.276\text{C} / \text{m}^2$	$e_{24} = e_{42} = -0.45\text{C} / \text{m}^2$
	$\epsilon_{11} = 1.1068 \times 10^{-8}\text{ F} / \text{m}$	$\epsilon_{11} = 7.77 \times 10^{-8}\text{ F} / \text{m}$
	$\epsilon_{22} = 1.1068 \times 10^{-8}\text{ F} / \text{m}$	$\epsilon_{22} = 7.77 \times 10^{-8}\text{ F} / \text{m}$
	$\epsilon_{33} = 1.1068 \times 10^{-8}\text{ F} / \text{m}$	$\epsilon_{33} = 8.91 \times 10^{-8}\text{ F} / \text{m}$
	$\rho_{\text{PVDF}} = 1780\text{kg} / \text{m}^3$	$\rho_{\text{ZnO}} = 5610\text{kg} / \text{m}^3$

Table 2. Comparison of the results for vibration ($\Omega_{\text{nonlocal}} / \Omega_{\text{local}}$) of the SLGS for all edges simply supported between the present study and Refs. (Pradhan & Kumar [11]; Shen et al [15]; Pradhan & Phadikar [17])

$(e_0 a)^2\text{ (nm)}^2$	Pradhan and Kumar [11]	Shen et al [15]	Pradhan and Phadikar [17]	Present work
0	1	1	1	1
1	0.9139	0.9139	0.9139	0.9139
2	0.8468	0.8467	0.8467	0.8467
3	0.7926	0.7925	0.7925	0.7925

6.2 Results

Nondimensional critical buckling load according to the variations of external electric voltage for various values of nonlocal parameter is shown in Fig. 3. In the figure, two main parameters for the behavior of critical buckling load are investigated. As it is indicative in the figure, nondimensional critical buckling load increases when the external electric voltage rises, and decreases when the value of nonlocal parameter increments.

Nondimensional critical buckling load according to nonlocal parameter for various biaxial compression ratios is indicated in Fig. 4. The figure shows that nondimensional critical buckling load has the maximum value when it is under uniaxial pressure ($q=0$), and it reduces when loading ratio increases.

In Fig. 5, nondimensional critical buckling load according to nonlocal parameter for various ratios of width to thickness of Graphene is shown. As indicated in the figure, nondimensional critical buckling load rises when the ratio of width to thickness of Graphene increases.

The effect of nonlocal parameter on nondimensional critical buckling load for various values of Winkler spring stiffness is shown in Fig. 6. In the figure, it is observable that nondimensional critical buckling load grows up when Winkler spring stiffness increases, since the stiffness of elastic medium increases when Winkler spring stiffness rises, and the stiffness of the system increases by incrementing the stiffness of elastic medium and, consequently, nondimensional critical buckling load enhances. Nondimensional critical buckling load according to nonlocal parameter for PVDF and ZnO material is shown in Fig. 7. As observable in the figure, nondimensional critical buckling load is higher for PVDF than that for ZnO material. The schematic representation of the buckling mode for a system under biaxial pressure for different buckling modes is shown in Fig. 8.

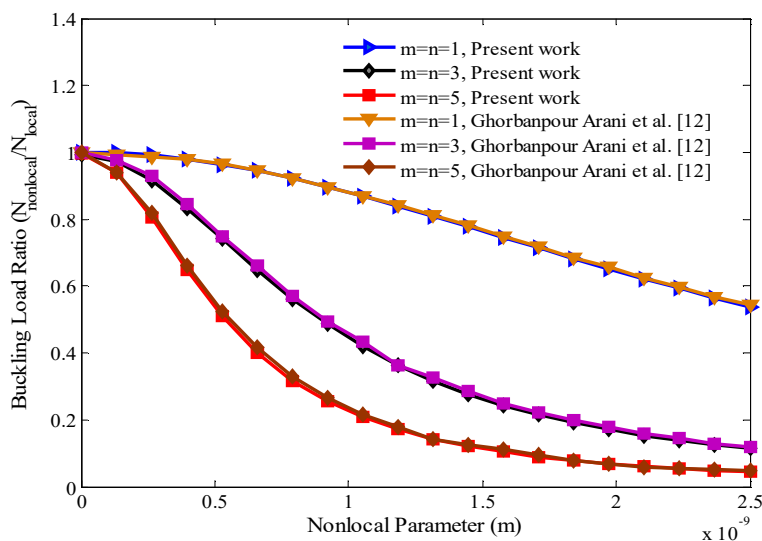


Fig. 2. Comparison of buckling load ratios for SLGS coupled with PVDF nanoplate according to nonlocal parameter, $m=n=1$, $m=n=3$, $m=n=5$



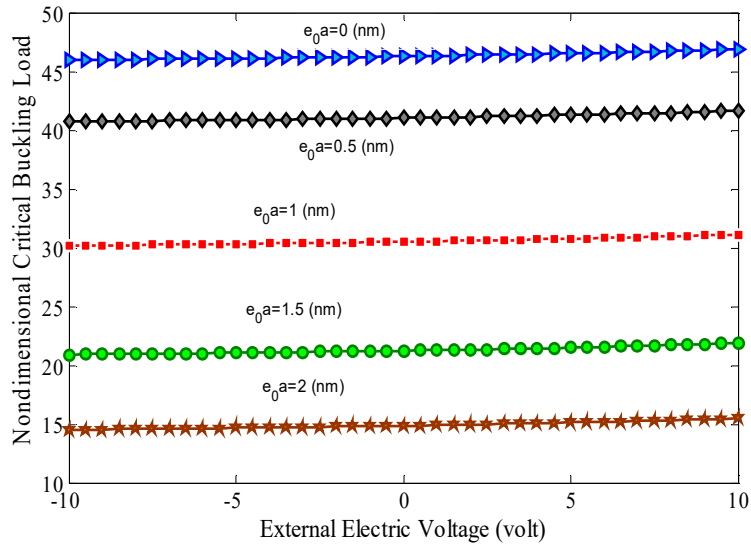


Fig. 3. Effect of nonlocal parameter on nondimensional critical buckling load for different nonlocal parameters

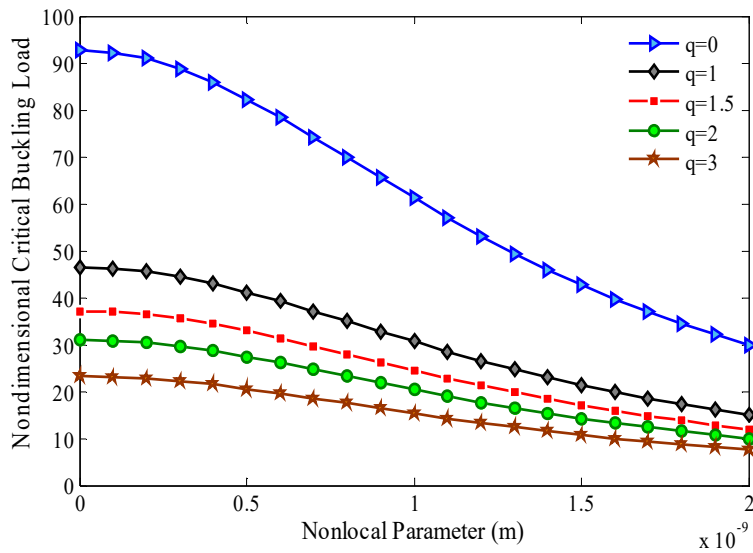


Fig. 4. Effect of nonlocal parameter on nondimensional critical buckling load for different biaxial compression ratios

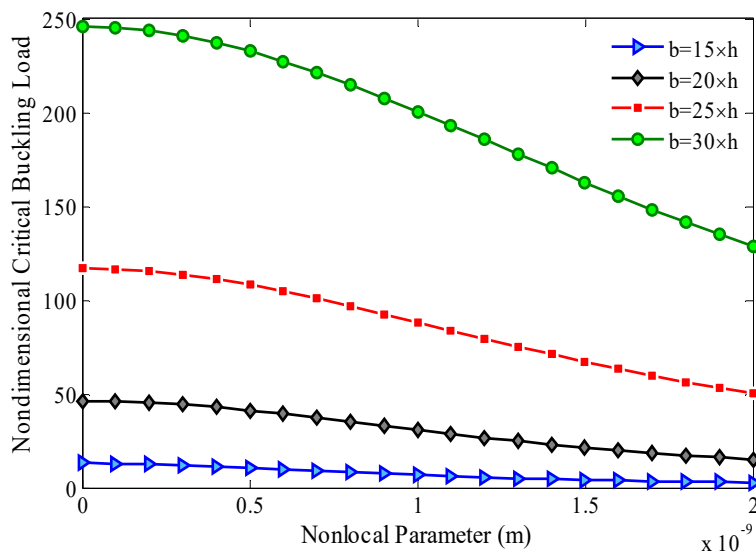


Fig. 5. Effect of nonlocal parameter on nondimensional critical buckling load for width to thickness of Graphene ratios



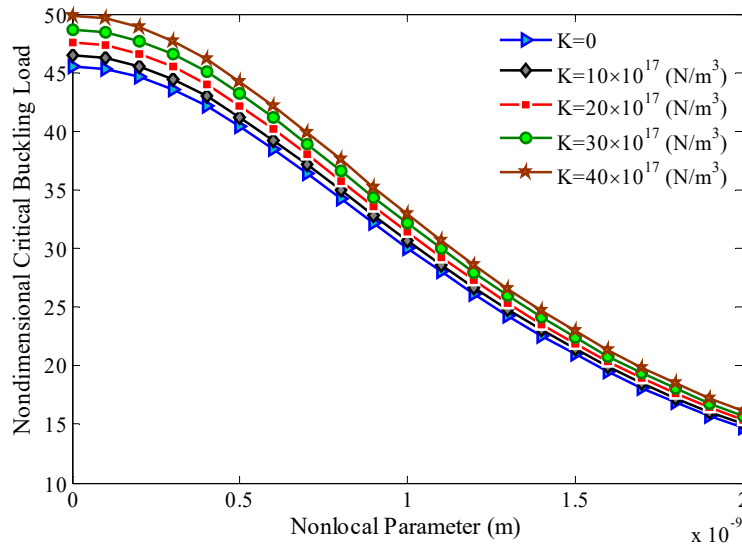


Fig. 6. Effect of nonlocal parameter on nondimensional critical buckling load for different values of Winkler spring stiffness

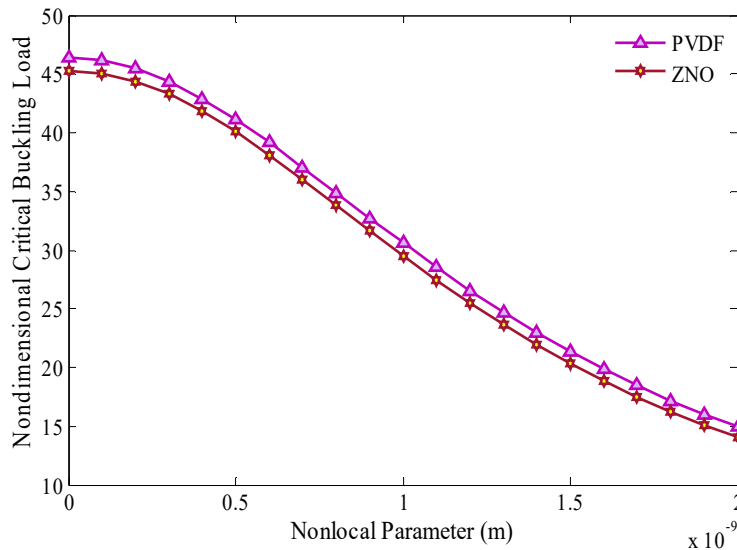


Fig. 7. Effect of nonlocal parameter on nondimensional critical buckling load considering two different piezoelectric nanoplates of PVDF and ZnO

Figure 9 indicates the effect of nonlocal parameter on nondimensional frequency of the system considering two piezoelectric PVDF and ZnO nanoplates. As observable in the figure, nonlocal frequency causes reduction in nondimensional frequency, and when nonlocal frequency enhances, nondimensional frequency of the system reduces more while considering ZnO than PVDF. Although, the value of nondimensional frequency of the system for ZnO is higher initially, but after $e_0 \bar{a} \cong 0.74 \text{ nm}$, the value of nondimensional frequency becomes less for ZnO material than that for PVDF material.

Nonlocal frequency of the system for different vibration modes according to various ratios of length to width for different values of nonlocal parameter are listed in Tables 3 and 4, considering PVDF and ZnO, respectively. Analyzing the results of the two tables indicates that the nonlocal frequency of the system enhances by increasing the number of vibration mode and the ratio of length to width. Comparing the two tables, it can be found out that the nonlocal parameter causes more reduction in the magnitude of nondimensional frequency of the system, while considering ZnO rather than PVDF, and also, when the ratio of length to width enhances, the nondimensional frequency of the system increases, while considering ZnO rather than PVDF for the local state and increases by incrementing nonlocal parameter for PVDF comparing to ZnO (since nonlocal parameter has more reduction effect for ZnO than PVDF), and it is observable in Fig. 9.

Nondimensional frequency of the system for different vibration modes according to various ratios of width to thickness of Graphene for different values of external electric voltage are listed in Tables 5 and 6, considering PVDF and ZnO, respectively. Analyzing the results of the two tables, it is shown that the nondimensional frequency of the system rises when the ratio of width to thickness enhances and decreases when the external electric voltage increases. Comparing the two tables indicates that for the ratio of $b/h=15$, nondimensional frequency of the system while considering PVDF is less than that while considering ZnO, and the value of nondimensional frequency of the system becomes more while considering PVDF comparing to ZnO, when the ratio of width to thickness rises.



Table 3. Nondimensional frequency for different vibration modes according to various length to width ratios for different nonlocal parameters considering PVDF

$b = 20 \times h, V_0 = 2 \text{ volt}, K = 8.9995035 \times 10^{17} \text{ Gpa / nm}, G = 2.71273 \text{ N / m}$

(m,n)	a/b	$e_0 \bar{a} (\text{nm})$				
		0	0.5	1	1.5	2
(1,1)	1	5.2148	5.1059	4.8761	4.6677	4.5369
	1.5	9.6627	9.5569	9.3171	9.0756	8.9049
	2	15.8276	15.7063	15.4246	15.1309	14.9167
	3	33.5368	33.3474	32.8997	32.4209	32.0640
(2,1)	1	9.2118	8.5856	7.6797	6.7177	5.3974
	1.5	14.3314	13.8380	12.8945	12.1578	11.7837
	2	20.8594	20.4237	19.5044	18.6709	18.1475
	3	38.6508	38.2277	37.2685	36.3025	35.6194
(2,2)	1	11.0296	10.3737	10.2026	8.7551	6.8847
	1.5	18.8379	17.8215	16.7867	16.6909	16.6674
	2	29.8325	28.4656	26.8225	26.7482	26.5797
	3	61.2005	58.7864	55.5865	54.9917	53.8081

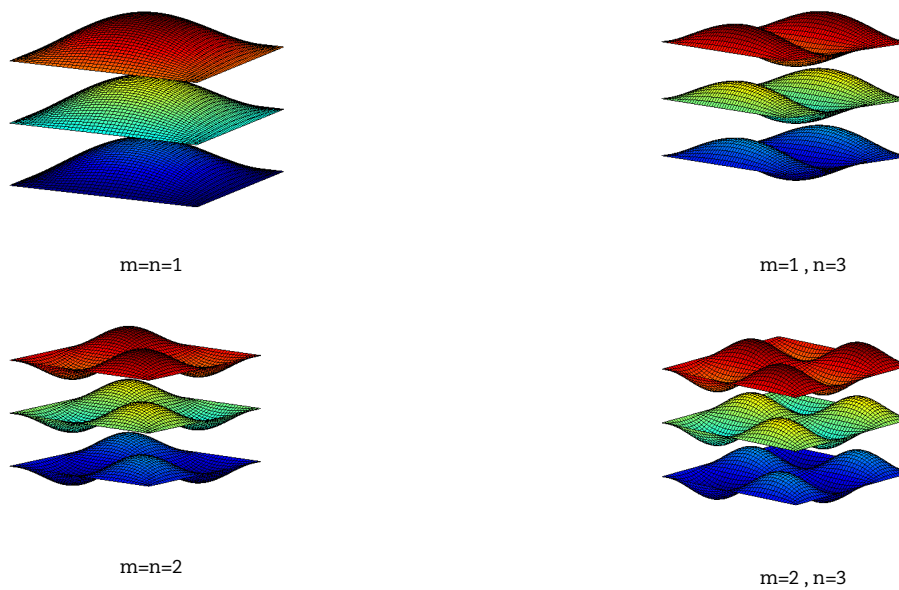


Fig. 8. Mode shapes for a system subjected to biaxial compression

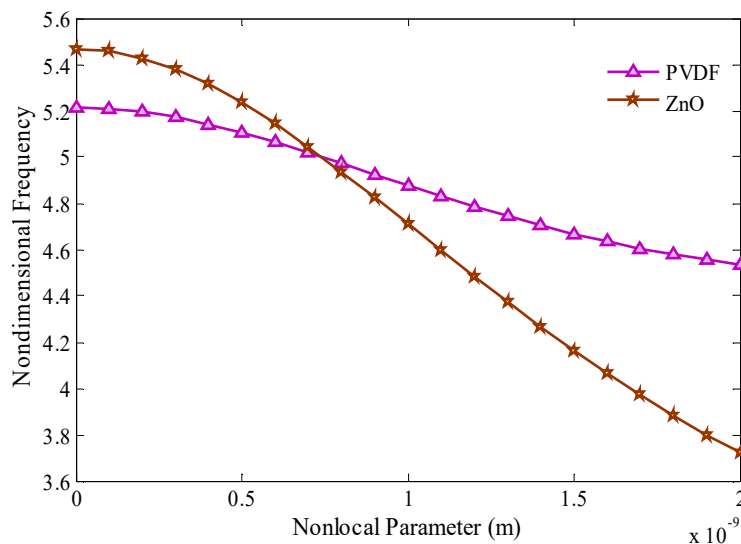


Fig. 9. Effect of nonlocal parameter on nondimensional frequency considering two different piezoelectric nanoplates of PVDF and ZnO

Nondimensional frequency of the system according to nonlocal parameters considering the elastic medium (Winkler and Pasternak models) and also without considering Winkler and Pasternak models, is shown in Figure 10. The figure shows that the stiffness of the system is higher while considering both models (Winkler and Pasternak) rather than only considering Pasternak model, and while only Winkler model is under consideration, the stiffness of the system is less than that in the two other states. Thus, the nondimensional frequency of the system is higher while considering both Winkler and Pasternak models comparing to that in the two other states, and it is higher while only considering Pasternak rather than Winkler model. Therefore, it can be concluded that the stiffness of the system is directly related to nondimensional frequency of the system.



Table 4. Nondimensional frequency for different vibration modes according to various length to width ratios for different nonlocal parameters considering ZnO for $b = 20 \times h$, $V_0 = 2$ volt, $K = 8.9995035 \times 10^{17}$ Gpa / nm, $G = 2.71273$ N / m

(m,n)	a/b	$e_0 \bar{a}$ (nm)				
		0	0.5	1	1.5	2
(1,1)	1	5.4681	5.2351	4.7103	4.1634	3.7211
	1.5	9.7821	9.4903	8.7872	7.9822	7.2691
	2	15.9067	15.5010	14.4983	13.3057	12.2077
	3	33.5826	32.8246	30.9152	28.4367	25.2273
(2,1)	1	10.7671	9.6457	7.7667	6.1486	4.9401
	1.5	15.7482	14.8031	12.8479	11.0232	9.6933
	2	21.8724	20.9406	18.8413	16.6537	14.8845
	3	39.1283	37.9611	35.1489	31.9286	29.0764
(2,2)	1	14.5976	12.4388	9.8231	7.9140	5.5801
	1.5	26.5049	23.4072	18.5697	15.4895	13.3508
	2	43.1049	38.6128	31.0812	24.5945	19.7605
	3	70.4314	63.3218	50.4546	39.7820	32.1657

Table 5. Nondimensional frequency for different vibration modes according to various width to thickness of Graphene ratios for different external electric voltages considering PVDF for $a = b$, $e_0 \bar{a} = 1$ nm, $K = 8.9995035 \times 10^{17}$ Gpa / nm, $G = 2.71273$ N / m

(m,n)	b/h	V_0				
		-2	-1	0	1	2
(1,1)	15	3.6518	3.6017	3.5510	3.4995	3.4471
	20	5.1589	5.0897	5.0195	4.9483	4.8761
	25	6.8497	6.7637	6.6766	6.5883	6.4988
	30	8.7481	8.6478	8.5463	8.4436	8.3396
(2,1)	15	4.1795	4.1055	4.0258	3.9401	3.8497
	20	8.0880	7.9882	7.8869	7.7841	7.6797
	25	10.4031	10.2717	10.1385	10.0034	9.8664
	30	12.9577	12.7992	12.6387	12.4760	12.3112
(2,2)	15	4.9217	4.8154	4.7065	4.5946	4.4798
	20	10.5029	10.4279	10.3528	10.2777	10.2026
	25	11.9796	11.8243	11.6668	11.5071	11.3452
	30	14.6071	14.4069	14.2039	13.9978	13.7886

Table 6. Nondimensional frequency for different vibration modes according to various width to thickness of Graphene ratios for different external electric voltages considering ZnO for $a = b$, $e_0 \bar{a} = 1$ nm, $K = 8.9995035 \times 10^{17}$ Gpa / nm, $G = 2.71273$ N / m

(m,n)	b/h	V_0				
		-2	-1	0	1	2
(1,1)	15	3.8742	3.8197	3.7645	3.7084	3.6514
	20	5.0449	4.9634	4.8805	4.7962	4.7103
	25	6.0722	5.9598	5.8453	5.7286	5.6093
	30	7.0742	6.9297	6.7821	6.6312	6.4768
(2,1)	15	4.8155	4.7696	4.7105	4.6574	4.6014
	20	7.8868	7.7986	7.7054	7.5943	7.4867
	25	10.4026	10.2454	10.0858	9.9235	9.7585
	30	12.3217	12.1235	11.9219	11.7168	11.5080
(2,2)	15	6.2316	6.1274	6.0212	5.9129	5.8025
	20	10.2766	10.1642	10.0511	9.9374	9.8231
	25	12.8350	12.6643	12.4913	12.3157	12.1376
	30	15.4967	15.2789	15.0579	14.8335	14.6057

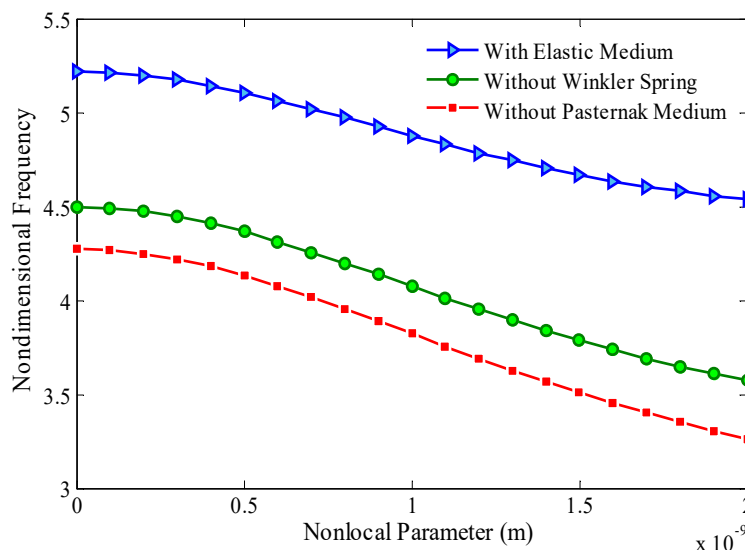


Fig. 10. Effect of nonlocal parameter on nondimensional frequency considering different types of elastic medium



7. Conclusions

Analyzing nanoplates in applying nanostructures and nanosystems has taken the attention of many researchers. In the present study, the buckling and vibration of a system composed of DLGS, where each layer is under van der Waals force with the other layer and under in-plane forces, coupled with a PVDF piezoelectric nanoplate through an elastic medium based on Winkler and Pasternak models and subjected to an external electric potential were investigated according to sinusoidal shear deformation theory of orthotropic plate extended with Eringen's nonlocal theory. Nondimensional frequency and critical buckling load were obtained using the Navier method for all edges with simply supported boundary conditions. Some results of the system were analyzed considering ZnO rather than PVDF nanoplate, and it was observed that nondimensional critical buckling load according to nonlocal parameter was less while considering ZnO rather than PVDF nanoplate. However, to compare a system with two different piezoelectric nanoplates of PVDF and ZnO, initially, the nondimensional frequency, according to the nonlocal parameter, increased, considering ZnO, and decreased after a while. In the present study, external electric voltage, loading ratios along y to x, ratio of width to the thickness and Winkler spring constant were discussed for nondimensional critical buckling load according to the nonlocal parameter, and ratio of length to width, external electric voltage, ratio of width to thickness, various vibration modes and the effect of elastic medium were presented for nondimensional frequency according to the nonlocal parameter. The results indicate that nondimensional frequency and nondimensional critical buckling load decreases when nonlocal parameter enhances, and when the external electric voltage increases, nondimensional frequency reduces and nondimensional critical buckling load rises, and nondimensional frequency and nondimensional critical buckling load increments when the effect of elastic medium and the ratio of width to thickness increases. Nondimensional frequency enhances when the number of modes and the ratio of length to width increases. Nondimensional critical buckling load is higher for the uniaxial than biaxial state, and nondimensional critical buckling load decreases when loading ratio along y to x enhances.

Author Contributions

All authors planned the scheme, initiated the project, developed the mathematical modeling and examined the theory validation. The manuscript was written through the contribution of all authors. All authors discussed the results, reviewed, and approved the final version of the manuscript.

Acknowledgments

Not applicable.

Conflict of Interest

The authors declared no potential conflicts of interest with respect to the research, authorship, and publication of this article.

Funding

The authors received no financial support for the research, authorship, and publication of this article.

Data Availability Statements

The datasets generated and/or analyzed during the current study are available from the corresponding author on reasonable request.

Nomenclature

μ	Small-scale effect (nm)	ρ	Mass density (kg / m^3)
u	Displacements at one point in the middle of a plate along the x (nm)	N_c	Critical buckling load (N)
v	Displacements at one point in the middle of a plate along the y (nm)	Ω	Natural frequency
w	Displacements at one point in the middle of a plate along the z (nm)	$[A]$	Stiffness matrix
ϕ_x	Rotations from the middle surface along the x-direction	$[M]$	Mass matrix
ϕ_y	Rotations from the middle surface along the y-direction	N_0	Nondimensional critical buckling load
h	The plate thickness (Graphene) (nm)	Ω_0	Nondimensional frequency
h_p	The plate thickness (piezoelectric) (nm)	V_0	External electric voltage (volt)
C_{ij}^p	Elastic coefficients (Graphene) (Gpa)	c	van der Waals coefficient (Gpa/nm)
C_{ij}^p	Elastic coefficients (piezoelectric) (Gpa)	a	Length (nm)
E_i	Young's modules ($i=1,2, 3$) (Gpa)	b	Width (nm)
G_{ij}	Shear modules ($i, j=1, 2, 3$ and $i \neq j$) (Gpa)	K	Winkler spring stiffness (Gpa/nm)
ν_{ij}	Poisson ratios ($i, j=1, 2, 3$ and $i \neq j$)	G	Pasternak shear modulus (N/m)
e_{ij}	Piezoelectric coefficients (C/m^2)	ϵ_{ii}	Dielectric coefficients (F/m)

Appendix

The elements of $[A]$ and $[M]$ are obtained by deriving δu_i , δv_i , δw_i , $\delta \phi_{ix}$ and $\delta \phi_{iy}$ ($i=1, 2, 3$) coefficients in the left and right sides of (23) to (34) eqs., respectively.

$$\delta u_i : \left[hC_{11} \right] u_{,mn} \left(\frac{m}{a} \right)^2 + \left[C_{66} h \right] u_{,mn} \left(\frac{n}{b} \right)^2 + \left[hC_{12} + C_{66} h \right] v_{,mn} \left(\frac{mn}{ab} \right) = I_{0G} u_{,mn} \Omega^2 \left\{ 1 + \mu \left[\left(\frac{n}{b} \right)^2 + \left(\frac{m}{a} \right)^2 \right] \right\} \quad (i = 1, 2) \quad (23)$$



$$\delta v_i : [C_{66}h]v_{imn} \left(\frac{m}{a}\right)^2 + [hC_{22}]v_{imn} \left(\frac{n}{b}\right)^2 + [C_{66}h + hC_{21}]u_{imn} \left(\frac{mn}{ab}\right) = I_{0G}v_{imn}\Omega^2 \left\{1 + \mu \left[\left(\frac{n}{b}\right)^2 + \left(\frac{m}{a}\right)^2\right]\right\} \quad (i = 1, 2) \tag{24}$$

$$\delta w_1 : \left[\frac{h^3}{12}C_{11} + \mu\gamma_1N_{cr}\right]w_{1mn} \left(\frac{m\pi}{a}\right)^4 + \left[\frac{h^3}{12}C_{22} + \mu\gamma_2N_{cr}\right]w_{1mn} \left(\frac{n\pi}{b}\right)^4 + \left[\frac{h^3}{6}C_{12} + \frac{h^3C_{66}}{3} + \mu\gamma_1N_{cr} + \mu\gamma_2N_{cr}\right]w_{1mn} \left(\frac{m^2n^2\pi^4}{a^2b^2}\right) - \left[\frac{2h^3}{\pi^3}C_{11}\right]\phi_{1xmn} \left(\frac{m\pi}{a}\right)^3 - \left[\frac{2h^3}{\pi^3}C_{22}\right]\phi_{1ymn} \left(\frac{n\pi}{b}\right)^3 - \left[\frac{2h^3}{\pi^3}C_{12} + \frac{4h^3C_{66}}{\pi^3}\right]\phi_{1ymn} \left(\frac{m^2n\pi^3}{a^2b}\right) - \left[\frac{2h^3}{\pi^3}C_{21} + \frac{4h^3C_{66}}{\pi^3}\right]\phi_{1xmn} \left(\frac{mn^2\pi^3}{ab^2}\right) \tag{25}$$

$$\delta w_2 : +[\gamma_1N_{cr} - c_{12}\mu]w_{1mn} \left(\frac{m\pi}{a}\right)^2 + [\gamma_2N_{cr} - c_{12}\mu]w_{1mn} \left(\frac{n\pi}{b}\right)^2 + c_{12}\mu w_{2mn} \left(\frac{m\pi}{a}\right)^2 + c_{12}\mu w_{2mn} \left(\frac{n\pi}{b}\right)^2 - c_{12}(w_{1mn} - w_{2mn}) = I_{0G}w_{1mn}\Omega^2 \left\{1 + \mu \left[\left(\frac{n\pi}{b}\right)^2 + \left(\frac{m\pi}{a}\right)^2\right]\right\} + I_{2G}w_{1mn}\Omega^2 \left[\left(\frac{n\pi}{b}\right)^2 + \left(\frac{m\pi}{a}\right)^2\right] \left\{1 + \mu \left[\left(\frac{n\pi}{b}\right)^2 + \left(\frac{m\pi}{a}\right)^2\right]\right\} - J_{1G}\phi_{1ymn}\Omega^2 \left(\frac{n\pi}{b}\right) \left\{1 + \mu \left[\left(\frac{n\pi}{b}\right)^2 + \left(\frac{m\pi}{a}\right)^2\right]\right\} - J_{1G}\phi_{1xmn}\Omega^2 \left(\frac{m\pi}{a}\right) \left\{1 + \mu \left[\left(\frac{n\pi}{b}\right)^2 + \left(\frac{m\pi}{a}\right)^2\right]\right\} \tag{26}$$

$$\delta \phi_{ix} : \left[-\frac{2h^3}{\pi^3}C_{11}\right]w_{imn} \left(\frac{m\pi}{a}\right)^3 + \left[-\frac{2h^3}{\pi^3}C_{12} - \frac{4h^3C_{66}}{\pi^3}\right]w_{imn} \left(\frac{mn^2\pi^3}{ab^2}\right) + \left[\frac{h^3}{2\pi^2}C_{11}\right]\phi_{ixmn} \left(\frac{m\pi}{a}\right)^2 + \left[\frac{h^3}{2\pi^2}C_{12} + \frac{h^3C_{66}}{2\pi^2}\right]\phi_{iymn} \left(\frac{mn\pi^2}{ab}\right) + \left[\frac{h^3C_{66}}{4\pi^2}\right]\phi_{ixmn} \left(\frac{n\pi}{b}\right)^2 + \frac{C_{55}h}{2}\phi_{ixmn} = -J_{1G}w_{imn}\Omega^2 \left(\frac{m\pi}{a}\right) \left\{1 + \mu \left[\left(\frac{n\pi}{b}\right)^2 + \left(\frac{m\pi}{a}\right)^2\right]\right\} + K_{0G}\phi_{ixmn}\Omega^2 \left\{1 + \mu \left[\left(\frac{n\pi}{b}\right)^2 + \left(\frac{m\pi}{a}\right)^2\right]\right\} \quad (i = 1, 2) \tag{27}$$

$$\delta \phi_{iy} : \left[-\frac{2h^3}{\pi^3}C_{22}\right]w_{imn} \left(\frac{n\pi}{b}\right)^3 + \left[-\frac{2h^3}{\pi^3}C_{21} - \frac{4h^3C_{66}}{\pi^3}\right]w_{imn} \left(\frac{m^2n\pi^3}{a^2b}\right) + \left[\frac{h^3C_{66}}{2\pi^2}\right]\phi_{iymn} \left(\frac{m\pi}{a}\right)^2 + \left[\frac{h^3}{2\pi^2}C_{21} + \frac{h^3C_{66}}{2\pi^2}\right]\phi_{ixmn} \left(\frac{mn\pi^2}{ab}\right) + \left[\frac{h^3}{2\pi^2}C_{22}\right]\phi_{iymn} \left(\frac{n\pi}{b}\right)^2 + \frac{C_{44}h}{2}\phi_{iymn} = -J_{1G}w_{imn}\Omega^2 \left(\frac{n\pi}{b}\right) \left\{1 + \mu \left[\left(\frac{n\pi}{b}\right)^2 + \left(\frac{m\pi}{a}\right)^2\right]\right\} + K_{0G}\phi_{iymn}\Omega^2 \left\{1 + \mu \left[\left(\frac{n\pi}{b}\right)^2 + \left(\frac{m\pi}{a}\right)^2\right]\right\} \tag{28}$$

$$\delta u_3 : [h_p C_{11}^p]u_{3mn} \left(\frac{m}{a}\right)^2 + [C_{66}^p h_p]u_{3mn} \left(\frac{n}{b}\right)^2 + [h_p C_{12}^p + C_{66}^p h_p]u_{3mn} \left(\frac{mn}{ab}\right) = I_{0P}u_{3mn}\Omega^2 \left\{1 + \mu \left[\left(\frac{n}{b}\right)^2 + \left(\frac{m}{a}\right)^2\right]\right\} \tag{29}$$

$$\delta v_3 : [C_{66}^p h_p]v_{3mn} \left(\frac{m}{a}\right)^2 + [h_p C_{22}^p]v_{3mn} \left(\frac{n}{b}\right)^2 + [C_{66}^p h_p + h_p C_{21}^p]u_{3mn} \left(\frac{mn}{ab}\right) = I_{0P}v_{3mn}\Omega^2 \left\{1 + \mu \left[\left(\frac{n}{b}\right)^2 + \left(\frac{m}{a}\right)^2\right]\right\} \tag{30}$$

$$\delta w_3 : \left[\frac{h_p^3}{12}C_{11}^p + G_{32}\mu + 2\mu e_{13}V_0\right]w_{3mn} \left(\frac{m\pi}{a}\right)^4 + \left[\frac{h_p^3}{12}C_{22}^p + G_{32}\mu + 2\mu e_{23}V_0\right]w_{3mn} \left(\frac{n\pi}{b}\right)^4 + \left[\frac{h_p^3}{6}C_{12}^p + \frac{h_p^3C_{66}^p}{2} + 2G_{32}\mu + 2\mu e_{13}V_0 + 2\mu e_{23}V_0\right]w_{3mn} \left(\frac{m^2n^2\pi^4}{a^2b^2}\right) - \left[\frac{2h_p^3}{\pi^3}C_{11}^p\right]\phi_{3xmn} \left(\frac{m\pi}{a}\right)^3 - \left[\frac{2h_p^3}{\pi^3}C_{22}^p\right]\phi_{3ymn} \left(\frac{n\pi}{b}\right)^3 - \left[\frac{2h_p^3}{\pi^3}C_{12}^p + \frac{4h_p^3C_{66}^p}{\pi^3}\right]\phi_{3ymn} \left(\frac{m^2n\pi^3}{a^2b}\right) - \left[\frac{2h_p^3}{\pi^3}C_{21}^p + \frac{4h_p^3C_{66}^p}{\pi^3}\right]\phi_{3xmn} \left(\frac{mn^2\pi^3}{ab^2}\right) + \left[\frac{2h_p e_{31}}{\pi}\right]\varphi_{mn} \left(\frac{m\pi}{a}\right)^2 + \left[\frac{2h_p e_{32}}{\pi}\right]\varphi_{mn} \left(\frac{n\pi}{b}\right)^2 + [G_{32} + 2e_{13}V_0 + K_{32}\mu]w_{3mn} \left(\frac{m\pi}{a}\right)^2 + [G_{32} + 2e_{23}V_0 + K_{32}\mu]w_{3mn} \left(\frac{n\pi}{b}\right)^2 - [G_{32} + K_{32}\mu]w_{2mn} \left(\frac{m\pi}{a}\right)^2 - [G_{32} + K_{32}\mu]w_{2mn} \left(\frac{n\pi}{b}\right)^2 - G_{32}\mu w_{2mn} \left(\frac{m\pi}{a}\right)^4 - 2G_{32}\mu w_{2mn} \left(\frac{m^2n^2\pi^4}{a^2b^2}\right) - G_{32}\mu w_{2mn} \left(\frac{n\pi}{b}\right)^4 + K_{32}(w_{3mn} - w_{2mn}) = I_{0P}w_{3mn}\Omega^2 \left\{1 + \mu \left[\left(\frac{n\pi}{b}\right)^2 + \left(\frac{m\pi}{a}\right)^2\right]\right\} + I_{2PP}w_{3mn}\Omega^2 \left[\left(\frac{n\pi}{b}\right)^2 + \left(\frac{m\pi}{a}\right)^2\right] \left\{1 + \mu \left[\left(\frac{n\pi}{b}\right)^2 + \left(\frac{m\pi}{a}\right)^2\right]\right\} - J_{1P}\phi_{3ymn}\Omega^2 \left(\frac{n\pi}{b}\right) \left\{1 + \mu \left[\left(\frac{n\pi}{b}\right)^2 + \left(\frac{m\pi}{a}\right)^2\right]\right\} - J_{1P}\phi_{3xmn}\Omega^2 \left(\frac{m\pi}{a}\right) \left\{1 + \mu \left[\left(\frac{n\pi}{b}\right)^2 + \left(\frac{m\pi}{a}\right)^2\right]\right\} \tag{31}$$

$$\delta \phi_{3x} : \left[-\frac{2h_p^3}{\pi^3}C_{11}^p\right]w_{3mn} \left(\frac{m\pi}{a}\right)^3 + \left[-\frac{2h_p^3}{\pi^3}C_{12}^p - \frac{4h_p^3C_{66}^p}{\pi^3}\right]w_{3mn} \left(\frac{mn^2\pi^3}{ab^2}\right) + \left[\frac{h_p^3}{2\pi^2}C_{11}^p\right]\phi_{3xmn} \left(\frac{m\pi}{a}\right)^2 + \left[\frac{h_p^3}{2\pi^2}C_{12}^p + \frac{h_p^3C_{66}^p}{2\pi^2}\right]\phi_{3ymn} \left(\frac{mn\pi^2}{ab}\right) + \left[\frac{h_p^3C_{66}^p}{2\pi^2}\right]\phi_{3xmn} \left(\frac{n\pi}{b}\right)^2 + \frac{C_{55}^p h_p}{2}\phi_{3xmn} + \left[-\frac{e_{15}h_p}{2} + \frac{e_{31}h_p}{2}\right]\varphi_{mn} \left(\frac{m\pi}{a}\right) = -J_{1P}w_{3mn}\Omega^2 \left(\frac{m\pi}{a}\right) \left\{1 + \mu \left[\left(\frac{n\pi}{b}\right)^2 + \left(\frac{m\pi}{a}\right)^2\right]\right\} + K_{0P}\phi_{3xmn}\Omega^2 \left\{1 + \mu \left[\left(\frac{n\pi}{b}\right)^2 + \left(\frac{m\pi}{a}\right)^2\right]\right\} \tag{32}$$



$$\delta\phi_{3y} : \left[-\frac{2h_p^3}{\pi^3} C_{22}^p \right] w_{3mn} \left(\frac{n\pi}{b} \right)^3 + \left[-\frac{2h_p^3}{\pi^3} C_{21}^p - \frac{4h_p^3 C_{66}^p}{\pi^3} \right] w_{3mn} \left(\frac{m^2 n \pi^3}{a^2 b} \right) + \left[\frac{h_p^3 C_{66}^p}{2\pi^2} \right] \phi_{3ymn} \left(\frac{m\pi}{a} \right)^2 + \left[\frac{h_p^3}{2\pi^2} C_{21}^p + \frac{h_p^3 C_{66}^p}{2\pi^2} \right] \phi_{3xmn} \left(\frac{mn\pi^2}{ab} \right) + \left[\frac{h_p^3}{2\pi^2} C_{22}^p \right] \phi_{3ymn} \left(\frac{n\pi}{b} \right)^2 + \frac{C_{44}^p h_p}{2} \phi_{3ymn} + \left[-\frac{e_{24} h_p}{2} + \frac{e_{32} h_p}{2} \right] \varphi_{mn} \left(\frac{n\pi}{b} \right) = -J_{1p} w_{3mn} \Omega^2 \left(\frac{n\pi}{b} \right) \left\{ 1 + \mu \left[\left(\frac{n\pi}{b} \right)^2 + \left(\frac{m\pi}{a} \right)^2 \right] \right\} + K_{0p} \phi_{3ymn} \Omega^2 \left\{ 1 + \mu \left[\left(\frac{n\pi}{b} \right)^2 + \left(\frac{m\pi}{a} \right)^2 \right] \right\} \quad (33)$$

$$\delta\varphi : \left[\frac{e_{15} h_p}{2} + \frac{e_{31} h_p}{2} \right] \phi_{3xmn} \left(\frac{m\pi}{a} \right) + \frac{e_{11} h_p}{2} \varphi_{mn} \left(\frac{m\pi}{a} \right)^2 + \left[\frac{e_{24} h_p}{2} + \frac{e_{32} h_p}{2} \right] \phi_{3ymn} \left(\frac{n\pi}{b} \right) + \frac{e_{22} h_p}{2} \varphi_{mn} \left(\frac{n\pi}{b} \right)^2 - \frac{2e_{31} h_p}{\pi} w_{3mn} \left(\frac{m\pi}{a} \right)^2 - \frac{2e_{32} h_p}{\pi} w_{3mn} \left(\frac{n\pi}{b} \right)^2 + \frac{e_{33} \pi^2}{2h_p} \varphi_{mn} = 0 \quad (34)$$


References


- [1] Hashemi S.H., Samaei A.T., Buckling analysis of micro/nanoscale plates via nonlocal elasticity theory. *Physica E: Low-dimensional Systems and Nanostructures*, 43, 2011, 1400-1404.
- [2] Murmu T., Pradhan S.C., Buckling of biaxially compressed orthotropic plates at small scales. *Mechanics Research Communications*, 36, 2009, 933-938.
- [3] Haghshenas A., Arani A.G., Nonlocal vibration of a piezoelectric polymeric nanoplate carrying nanoparticle via Mindlin plate theory. *Proceedings of the Institution of Mechanical Engineers, Part C: Journal of Mechanical Engineering Science*, 228, 2014, 907-920.
- [4] Jomehzadeh E., Saidi A.R., A study on large amplitude vibration of multilayered graphene sheets. *Computational Materials Science*, 50, 2011, 1043-1051.
- [5] Ghorbanpour Arani A., Fereidoon A., Kolahchi R., Nonlocal DQM for a nonlinear buckling analysis of DLGSs integrated with ZnO piezoelectric layers. *Journal of Computational Applied Mechanics*, 45, 2014, 9-22.
- [6] Cao Q., Xiao G., Huaipeng W., Pengjie W., Aaron L., Yucheng L., Qing P., A review of current development of graphene mechanics. *Crystals*, 8, 2018, 357.
- [7] Eringen A.C., On differential equations of nonlocal elasticity and solutions of screw dislocation and surface waves. *Journal of Applied Physics*, 54, 1983, 4703-4710.
- [8] Eringen A.C., Nonlocal polar elastic continua. *International Journal of Engineering Science*, 10, 1972, 1-16.
- [9] Eringen A.C., *Nonlocal continuum field theories*. New York, Springer, 2002.
- [10] Arani A.G., Shiravand, A., Rahi, M., Kolahchi, R., Nonlocal vibration of coupled DLGS systems embedded on Visco-Pasternak foundation. *Physica B: Condensed Matter*, 407, 2012, 4123-4131.
- [11] Pradhan S.C., Kumar A., Vibration analysis of orthotropic graphene sheets using nonlocal elasticity theory and differential quadrature method. *Composite Structures*, 93, 2011, 774-779.
- [12] Arani A.G., Kolahchi R., Vossough H., Buckling analysis and smart control of SLGS using elastically coupled PVDF nanoplate based on the nonlocal Mindlin plate theory. *Physica B: Condensed Matter*, 407, 2012, 4458-4465.
- [13] Ke L.L., Liu C., Wang Y.S., Free vibration of nonlocal piezoelectric nanoplates under various boundary conditions. *Physica E: Low-dimensional Systems and Nanostructures*, 66, 2015, 93-106.
- [14] Ebrahimi F., Barati M.R., Damping vibration analysis of smart piezoelectric polymeric nanoplates on viscoelastic substrate based on nonlocal strain gradient theory. *Smart Materials and Structures*, 26, 2017, 065018.
- [15] Shen Z.B., Tang H.L., Li D.K., Tang G.J., Vibration of single-layered graphene sheet-based nanomechanical sensor via nonlocal Kirchhoff plate theory. *Computational Materials Science*, 61, 2012, 200-205.
- [16] Malekzadeh P., Setoodeh A.R., Beni A.A., Small scale effect on the free vibration of orthotropic arbitrary straight-sided quadrilateral nanoplates. *Composite Structures*, 93, 2011, 1631-1639.
- [17] Pradhan S.C., Phadikar J.K., Nonlocal elasticity theory for vibration of nanoplates. *Journal of Sound and Vibration*, 325, 2009, 206-223.
- [18] Malikan M., Buckling analysis of a micro composite plate with nano coating based on the modified couple stress theory. *Journal of Applied and Computational Mechanics*, 4, 2018, 1-15.
- [19] Zhu X., Li, L., Twisting statics of functionally graded nanotubes using Eringen's nonlocal integral model. *Composite Structures*, 178, 2017, 87-96.
- [20] Zhu, X., Li, L., Longitudinal and torsional vibrations of size-dependent rods via nonlocal integral elasticity. *International Journal of Mechanical Sciences*, 133, 2017, 639-650.
- [21] Allahyari E., Asgari M., Thermo-mechanical vibration of double-layer graphene nanosheets in elastic medium considering surface effects; developing a nonlocal third order shear deformation theory. *European Journal of Mechanics-A/Solids*, 75, 2019, 307-321.
- [22] Kadari B., Bessaim A., Tounsi A., Heireche H., Bousahla A.A., Houari M.S.A., Buckling analysis of orthotropic nanoscale plates resting on elastic foundations. *International Journal of Nano Research*, 55, 2018, 42-56.
- [23] Shaat M., A general nonlocal theory and its approximations for slowly varying acoustic waves. *International Journal of Mechanical Sciences*, 130, 2017, 52-63.
- [24] Ghorbani K., Rajabpour A., Ghadiri M., Determination of carbon nanotubes size-dependent parameters: molecular dynamics simulation and nonlocal strain gradient continuum shell model. *Mechanics Based Design of Structures and Machines*, 2019, 1-18.
- [25] Thai H.T., Vo T.P., Nguyen T.K., Lee J., A nonlocal sinusoidal plate model for micro/nanoscale plates. *Proceedings of the Institution of Mechanical Engineers, Part C: Journal of Mechanical Engineering Science*, 228, 2014, 2652-2660.
- [26] Touratiar M., An efficient standard plate theory. *International Journal of Engineering Science*, 29, 1991, 901-916.
- [27] Khajehdehi Kavanroodi M., Fereidoon A., Mirafzal A.R., Buckling analysis of coupled DLGSs systems resting on elastic medium using sinusoidal shear deformation orthotropic plate theory. *Journal of the Brazilian Society of Mechanical Sciences and Engineering*, 39, 2017, 2817-2829.
- [28] Ghorbanpour Arani A., Jamali M., Ghorbanpour-Arani A.H., Kolahchi R., Mosayyebi M., Electro-magneto wave propagation analysis of viscoelastic sandwich nanoplates considering surface effects. *Proceedings of the Institution of Mechanical Engineers, Part C: Journal of Mechanical Engineering Science*, 231, 2017, 387-403.
- [29] Zenkour A.M., Sobhy M., Nonlocal elasticity theory for thermal buckling of nanoplates lying on Winkler-Pasternak elastic substrate medium. *Physica E: Low-dimensional Systems and Nanostructures*, 53, 2013, 251-259.
- [30] Chemi A., Zidour M., Heireche H., Rakrak K., Bousahla A.A., Critical buckling load of chiral double-walled carbon nanotubes embedded in an elastic medium. *Mechanics of Composite Materials*, 53, 2018, 827-836.
- [31] Narendar S., Gopalakrishnan S., Scale effects on buckling analysis of orthotropic nanoplates based on nonlocal two-variable refined plate theory. *Acta Mechanica*, 223, 2012, 395-413.
- [32] Lindahl N., Midtvedt D., Svensson J., Oleg A. Nerushev, Lindvall N., Isacson A., Eleanor EB Campbell, Determination of the bending rigidity of graphene via electrostatic actuation of buckled membranes. *Nano Letters*, 12, 2012, 3526-3531.
- [33] Pradhan S.C., Buckling of single layer graphene sheet based on nonlocal elasticity and higher order shear deformation theory. *Physics Letters A*, 373, 2009, 4182-4188.
- [34] Mohammadimehr M., Navi B.R., Arani A.G., Free vibration of viscoelastic double-bonded polymeric nanocomposite plates reinforced by FG-SWCNTs using MSGT, sinusoidal shear deformation theory and meshless method. *Composite Structures*, 131, 2015, 654-671.
- [35] Ansari R., Hasrati E., Faghih Shojaei M., Gholami R., Mohammadi V., Shahabodini A., Size-dependent bending, buckling and free vibration analyses of microscale functionally graded mindlin plates based on the strain gradient elasticity theory. *Latin American Journal of Solids and Structures*, 13, 2016, 632-664.





- [36] Farajpour A., Solghar A.A., Shahidi A., Postbuckling analysis of multi-layered graphene sheets under non-uniform biaxial compression. *Physica E: Low-dimensional Systems and Nanostructures*, 47, 2013, 197-206.
- [37] Arani A.G., Kolahchi R., Barzoki A.A.M., Mozdianfard M.R., Farahani S.M.N., Elastic foundation effect on nonlinear thermo-vibration of embedded double-layered orthotropic graphene sheets using differential quadrature method. *Proceedings of the Institution of Mechanical Engineers, Part C: Journal of Mechanical Engineering Science*, 227, 2013, 862-879.
- [38] Arani A.G., Abdollahian M., Kolahchi R., Nonlinear vibration of a nanobeam elastically bonded with a piezoelectric nanobeam via strain gradient theory. *International Journal of Mechanical Sciences*, 100, 2015, 32-40.
- [39] Mohammadimehr M., Rosta-Navi B., Ghorbanpour-Arani A., Biaxial buckling and bending of smart nanocomposite plate reinforced by CNTs using extended mixture rule approach. *Mechanics of Advanced Composite Structures*, 1, 2014, 17-26.
- [40] Thai H.T., Vo T.P., A new sinusoidal shear deformation theory for bending, buckling, and vibration of functionally graded plates. *Applied Mathematical Modeling*, 37, 2013, 3269-3281.
- [41] Mohammadimehr M., Mohandes M., Moradi M., Size dependent effect on the buckling and vibration analysis of double-bonded nanocomposite piezoelectric plate reinforced by boron nitride nanotube based on modified couple stress theory. *Journal of Vibration and Control*, 22, 2016, 1790-1807.
- [42] Xiang S., Wang J., Ai Y.T., Li G.C., Buckling analysis of laminated composite plates by using various higher-order shear deformation theories. *Mechanics of Composite Materials*, 51, 2015, 645-654.
- [43] Mohammadimehr M., Mohandes M., The effect of modified couple stress theory on buckling and vibration analysis of functionally graded double-layer boron nitride piezoelectric plate based on CPT. *Journal of Solid Mechanics*, 7, 2015, 281-298.
- [44] Kim S.E., Thai H.T., Lee J., Buckling analysis of plates using the two variable refined plate theory. *Thin-Walled Structures*, 47, 2009, 455-462.
- [45] Arani A.G., Jalaei M.H., Niknejad S., Arani, A.A.G., Size-Dependent Analysis of Orthotropic Mindlin Nanoplate on Orthotropic Visco-Pasternak Substrate with Consideration of Structural Damping. *Journal of Solid Mechanics*, 11, 2019, 236-253.

ORCID iD

K. Malekzadeh Fard  <https://orcid.org/0000-0002-4725-6949>

M. Khajehdehi Kavanroodi  <https://orcid.org/0000-0002-2691-0972>

H. Malek-Mohammadi  <https://orcid.org/0000-0001-7396-7480>

A.R. Pourmoayed  <https://orcid.org/0000-0002-7217-4582>



© 2022 Shahid Chamran University of Ahvaz, Ahvaz, Iran. This article is an open access article distributed under the terms and conditions of the Creative Commons Attribution-NonCommercial 4.0 International (CC BY-NC 4.0 license) (<http://creativecommons.org/licenses/by-nc/4.0/>).

How to cite this article: Malekzadeh Fard, K., Khajehdehi Kavanroodi, M., Malek-Mohammadi, H., Pourmoayed, A.R. Buckling and Vibration Analysis of a Double-layer Graphene Sheet Coupled with a Piezoelectric Nanoplate, *J. Appl. Comput. Mech.*, 8(1), 2022, 129-143. <https://doi.org/10.22055/JACM.2020.32145.1976>

Publisher's Note Shahid Chamran University of Ahvaz remains neutral with regard to jurisdictional claims in published maps and institutional affiliations.

